NATIONAL ADVISORY COMMITTEE FOR AERONAUTICS

TECHNICAL NOTE

No. 1204

EFFECT OF CENTRIFUGAL FORCE ON THE ELASTIC CURVE OF A VIBRATING CANTILEVER BEAM

By Scott H. Simpkinson, Laurel J. Eatherton
and Morton B. Millenson

Aircraft Engine Research Laboratory
Cleveland, Ohio

Washington
February 1947

NATIONAL ADVISORY COMMITTEE FOR AERONAUTICS

TECHNICAL NOTE NO. 1204

EFFECT OF CENTRIFUGAL FORCE ON THE ELASTIC CURVE OF A VIBRATING CANTILEVER BEAM

By Scott H. Simpkinson, Laurel J. Eatherton
and Morton B. Millenson

SUMMARY

A study was made to determine the effect of rotation on the dynamic-stress distribution in vibrating cantilever beams. The results of a mathematical analysis are presented together with experimental results obtained by means of stroboscopic photographs and strain gages. The theoretical analysis was confined to uniform cantilever beams; the experimental work was extended to include a tapered cantilever beam to simulate an aircraft propeller blade. Calculations were made on a nondimensional basis for second- and third-mode vibration; the experiments were carried out on beams of various lengths, materials, and cross sections for second-mode vibration. From this investigation it was concluded that high vibratory-stress positions are unaffected by the addition of centrifugal force at rotary speeds as high as 100 percent above the normal operating speed range of present aeronautical equipment. Nonrotating vibration surveys of blades therefore are valuable in predicting high vibratory-stress locations under operating conditions.

INTRODUCTION

Resonant vibration causes many of the failures encountered in aircraft propeller blades and in currently used high-speed compressor and turbine blades. The high stresses that cause these failures are brought about by the coincidence of one of the exciting forces present with one of the natural frequencies of the blade. Considerable progress was made on the study of resonant vibration with the introduction of strain gages for measuring stress in rotating parts. This method of measuring vibratory stress in propeller blades has become the standard procedure for determining safe engine-propeller combinations. The results obtained in this manner, however, have sometimes proved unsatisfactory because misleading data have resulted from the improper location of the strain gages. Many propeller-blade fatigue failures occurred on endurance test stands although the engine-propeller combination had been pronounced safe on the basis

of results obtained with strain-gage vibration surveys. Such failures indicate a need for a better method of locating strain gages on propeller blades. The strain gages could be properly located if the location of the high vibratory-stress positions can be determined.

The addition of centrifugal force causes a considerable change in the natural frequencies of a propeller blade. Reference 1 states and theoretical calculations in reference 2 imply that centrifugal force also changes the mode shapes and high-stress positions of a vibrating blade. British investigators (Morris and Head, and Piper) maintain, however, that centrifugal force has little or no effect on mode shape. If this opinion is correct, a static (nonrotating) vibration survey of a blade would result in the location of the high-stress positions for the various natural modes of vibration. Furthermore, only one static survey would be necessary for a particular type of blade, because geometrically similar blades have the same mode shapes and would therefore have geometrically similar high-stress positions.

In an effort to improve the checking of engine-propeller combinations and to provide a means of predicting vibration trouble in high-speed turbines and compressors, the NACA Cleveland laboratory conducted an investigation to determine the effect of centrifugal force on the mode shape and stress distribution of a rotating blade vibrating at resonance.

The vibration of uniform beams in a centrifugal-force field was mathemetically investigated employing a numerical method given by Myklestad (reference 3) for the determination of natural frequencies and mode shapes of such beams. The problem was experimentally studied by subjecting beams of various lengths and materials to rotational speeds up to 1015 rpm while vibrating in second mode. In addition to beams of uniform cross section, a beam of varying cross section, made to simulate a propeller blade, was also studied. Mode shapes were obtained from photographs taken using a stroboscopic light source and stress-distribution curves were obtained with strain gages. The results of the strain-gage data taken on the tapered beam (nonrotating) were compared with similar data obtained on a propeller blade to determine the similarity in properties of the tapered beam and of a propeller blade.

MATHEMATICAL PROCEDURE AND RESULTS

A convenient method of determining frequencies and mode shapes of rotating beams, such as propeller blades, helicopter rotors, and turbine blades, is given in reference 3. This method involves substituting a series of point masses and massless springs for the beam. The point masses are so selected that the mass distribution of the substitute system represents an approximation of the mass distribution of the actual beam. Similarly, the springs are selected to represent an approximation of the elastic distribution of the beam. Angular and linear deflections of each substitute spring, under the influence of unit loading and unit moment, are used as influence coefficients in the calculation. The method of calculation is analogous to the more commonly known Holzer method of analyzing torsional vibrations but is somewhat more complicated, particularly when the effect of centrifugal force is introduced. The calculation is made by assuming a natural frequency and computing the angular and linear deflections, point by point, proceeding from the free end of the beam to the fixed end. The assumed frequency is an actual natural frequency if the calculated deflections meet the end conditions at the fixed end. With skill the correct frequency can be determined after two or three calculations.

Although this method represents an approximation of actual conditions, the accuracy of the resulting values is limited only by the number of mass-spring sets used in approximating the beam. All the calculations for this investigation were made using 10 equal concentrated masses located at the midpoints of 10 equal sections of the beam. The accuracy of this approximation is shown in figure 1 where the second-mode deflection curves, calculated by the Myklestad method (reference 3) and by solution of the theoretical equation based on simple-beam theory given in reference 4, are plotted for a nonrotating uniform cantilever beam. The Myklestad method for this degree of approximation accurately determines the critical locations of the deflection curves; namely, the nodes, the antinodes, and the inflection points. Relative amplitudes, however, are somewhat in error.

A plot of the Myklestad calculation for a uniform cantilever beam vibrating in second mode, while rotating at a speed such that the ratio of angular velocity (radians/sec) to natural angular frequency (radians/sec) (ω/p) is 0.292, is shown in figure 2. A deflection curve of a cantilever beam with no rotation, as calculated from the theoretical equation of reference 4, is plotted on the same figure. Figure 3 shows the same type of plot for third-mode vibration. The Myklestad calculation for this figure

was made with $\omega/p = 0.160$. The two ratios, 0.292 (fig. 2) and 0.160 (fig. 3), represent angular velocities approximately 100 percent above the rotative speeds encountered in operation and were selected to emphasize any effect rotation might have on the location of critical points in the deflection curves.

Figure 2 indicates that no shift of critical points occurs because of rotation. The small shift in antinode positions in figure 3 is attributed to insufficient mass-spring combinations for accuracy at this higher mode of vibration.

APPARATUS AND TEST PROCEDURE

The experimental data were obtained with the apparatus (fig. 4), which included instruments for recording deflection, angular velocity, and vibration frequency. The setup provides a means of simultaneously vibrating and rotating a beam. A photoelectric tube, which actuated a stroboscope, was used to "stop" the beam for photographing the vibration during rotation. White dots were painted on the beam to facilitate photographing and measuring. The photoelectric-tube signal was also recorded on an oscillograph for use as a revolution counter. The signal from a vibration pickup located on the bedplate was impressed on another channel of the oscillograph as a simultaneous frequency counter. Strain gages, located as shown in figure 5, were used to obtain vibratory stress-distribution data.

Three different beams were used in the experiment. The first beam was of low-carbon steel with a cross section of 1 by $\frac{1}{16}$ inch and had a free length of $17\frac{13}{16}$ inches. The beam was mounted as a cantilever with the fixed end at the center of rotation. Various speeds from 0 to 1015 rpm were set with the variable-speed driving unit. The speed of the exciter was set for resonant second-mode vibration at each of the rotational speeds. A 30-second film exposure was made at each speed and records of the angular velocity and vibration frequency were obtained. The runs were then repeated with the beam enclosed in a transparent plastic box (fig. 6) to eliminate any effect of aerodynamic damping that might accompany combined rotation and vibration.

Strain gages were cemented to the top of the beam. The lead wires were cemented to the top of the beam and run to a slip-ring assembly having 13 channels. The signals from the strain gages

were impressed on a multichannel oscillograph capable of simultaneously recording 12 stresses. Records of the vibratory stress were obtained at speeds of 0, 536, and 1015 rpm at second-mode resonance.

The second beam was of soft brass with a cross section of 1 by $\frac{1}{8}$ inch and had a free length of 20 inches. Deflection photographs were taken of this beam at various angular velocities ranging from 0 to 998 rpm.

The third beam was of low-carbon steel with a cross section that varied uniformly from 1 by $\frac{3}{16}$ inch at the fixed end to 1 by $\frac{1}{64}$ inch at the free end. The free length of this tapered cantilever beam is $17\frac{3}{4}$ inches. The same type of frequency and mode-shape data were obtained for the tapered beam as for the uniform steel beam.

In order to obtain more complete data on the tapered beam, 18 strain gages were used. Because only 12 gage signals could be recorded at one time, the gages were wired into two groups of 12 gages each, the central six gages being common to both sets. One record of each set was taken at each test point. The data from the six common gages were used to correct for small changes in amplitude between readings.

A hollow steel propeller blade was so mounted as to be supported in the same manner as in an actual propeller hub. Strain gages were mounted on the camber side along the maximum camber line. Simultaneous records of bending stress along the blade were obtained with the propeller blade subjected to nonrotating second-mode vibration.

EXPERIMENTAL RESULTS

Photographs of the uniform cantilever steel beam, vibrating in second mode and rotating at speeds of 1015, 536, and 0 rpm, are shown in figure 7. Measurements were made from enlargements of these photographs and the data are plotted in figure 8. The only change in these curves resulting from an increase in speed of rotation is a decrease in relative antinode amplitude.

The experiment was then repeated with the beam enclosed in the transparent plastic box to eliminate any effects of rotational aerodynamic damping. When the results of measurements made from enlargements of the photographs shown in figure 9 were plotted, the

deflection curves were the same as those obtained with the unenclosed beam. It was therefore concluded that the effect of rotational aerodynamic damping could be neglected in the experiments.

Experimental vibratory stress-distribution curves for the uniform cantilever steel beam were obtained from the second derivatives of the deflection curves shown in figure 8. These stress-distribution curves, together with strain-gage readings, are shown in figure 10.

An accurate check of second-mode resonant frequency at various speeds of rotation was made. The frequency was assumed to vary with speed according to the formula derived from that given in reference 5

$$f = \sqrt{f_0^2 + K\Omega^2}$$

where

f resonant frequency, cycles per second

f_0 resonant frequency at 0 rpm, cycles per second

K constant

Ω angular velocity of beam, revolutions per second

The value of the constant K for second mode obtained from experimental data was 6.55 as compared with an approximate value of 6 given in reference 5. A comparison of curves obtained by using these two constants is given in figure 11.

In order to eliminate any coincidence involving the material constants or dimensions, a brass beam of different length and cross section was used in the second part of the experiment. Stroboscopic photographs of this beam are presented in figure 12. Deflection measurements made from enlargements of figure 12 are plotted in figure 13 and can be compared with the deflection curves of the uniform cantilever steel beam shown in figure 8. The identical nature of the two sets of deflection curves for the uniform cantilever brass and steel beams eliminated any necessity for a stress analysis of the brass beam. From these data, it is evident that the physical constants of the material or the dimensions have no effect on the elastic curve of a vibrating uniform cantilever beam. This conclusion is valid for both stationary and rotating beams.

Deflection curves for the tapered cantilever steel beam were obtained, as in the previous experiments, from the photographs shown in figure 14 and are presented in figure 15. The relation between antinode and tip deflection is considerably changed from the uniform cantilever-beam relation but the node occurs at the same place, that is, 78 percent of the length from the fixed end. The same tendency in antinode deflection compared with tip deflection occurs with increased angular velocity, as in the case of the uniform cantilever beam; that is, the antinode loop becomes smaller in relation to tip amplitude with increase in angular velocity of the beam. Stress distribution at a rotational speed of 0 rpm was obtained from the second derivative of the deflection curve (fig. 15(c)) and is plotted in figure 16 with the experimental points obtained from strain gages.

The tapered cantilever steel beam used in this experiment was so chosen as to represent a typical variation in cross-section moment of inertia along a propeller blade. In order to determine the degree of approximation of the tapered beam to a propeller blade, strain-gage measurements were made along the maximum camber line of a hollow steel propeller blade vibrating in second mode. These stress measurements are plotted in figure 16 together with the stress distribution of the tapered cantilever steel beam.

DISCUSSION

A comparison of the curves presented in figure 17, based on the results of both experiments and calculations, indicate that the introduction of centrifugal force has no effect on the maximum dynamic-stress locations in a vibrating cantilever beam fixed at the center of rotation within the investigated speed range. The general shape of the deflection curve, in particular the location of node positions, is also unaffected by rotation although relative amplitudes vary; that is, the amplitude of antinode loops relative to tip amplitude decreases with increasing rotational speed. Because node and maximum dynamic-stress locations are invariant, static-bending vibration surveys of beams that will be subsequently subjected to vibratory forces in a centrifugal-force field will locate critical areas for strain-gage location in rotary testing. This procedure will decrease the possibility of misleading data because of improperly located strain gages.

CONCLUSIONS

Two important conclusions may be drawn on the basis of the study of beams vibrating in a centrifugal-force field:

1. Node positions and maximum vibratory-stress locations are unaffected by centrifugal force within the investigated speed range in a cantilever beam fixed at the center of rotation and vibrating in bending modes.

2. Static-vibration surveys of propeller blades and similar rotating parts may be utilized to predict the maximum vibratory-stress positions in such blades under operating conditions.

Aircraft Engine Research Laboratory,
National Advisory Committee for Aeronautics,
Cleveland, Ohio, September 18, 1946.

REFERENCES

1. Theodorsen, T.: Propeller Vibrations and the Effect of Centrifugal Force. NACA TN No. 516, 1935.

2. Ramberg, Walter, and Levy, Sam: Calculation of Stresses and Natural Frequencies for a Rotating Propeller Blade Vibrating Flexurally. Res. Paper 1148, Nat. Bur. Standards Jour. Res., vol. 21, no. 5, Nov. 1938, pp. 639-669.

3. Myklestad, N. O.: Vibration Analysis. McGraw-Hill Book Co., Inc., 1944, pp. 210-214.

4. Timoshenko, S.: Vibration Problems in Engineering. D. Van Nostrand Co., Inc., 2d ed., 1937, pp. 331-345.

5. Den Hartog, J. P.: Mechanical Vibrations. McGraw-Hill Book Co., Inc., 2d ed., 1940, p. 310.

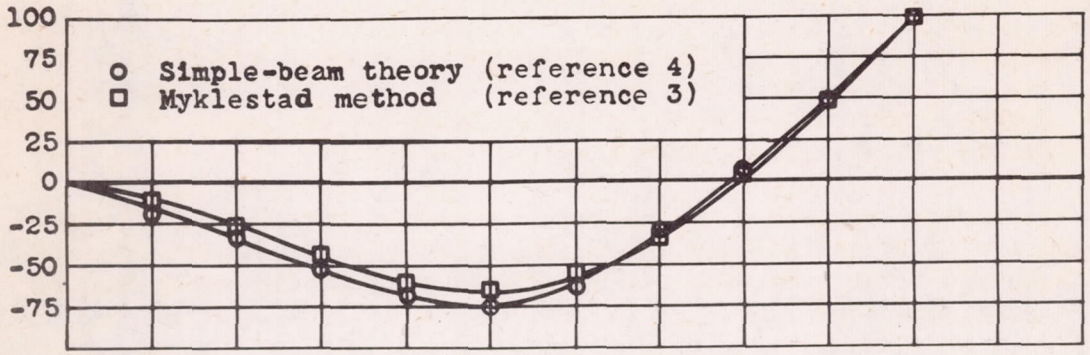

Figure 1. - Comparison of calculated second-mode deflection curves for nonrotating uniform cantilever beam.

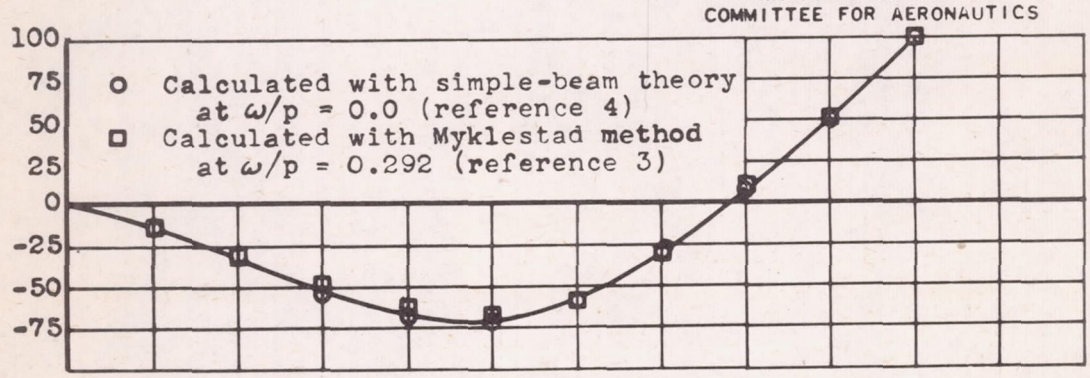

Figure 2. - Effect of centrifugal force on second-mode deflection curve of uniform cantilever beam.

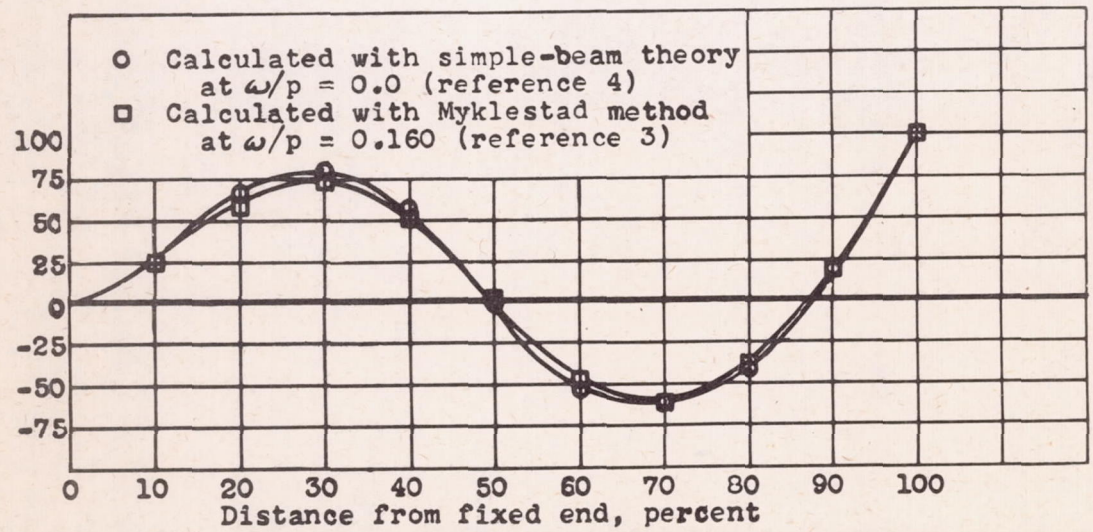

Figure 3. - Effect of centrifugal force on third-mode deflection curve of uniform-cantilever beam.

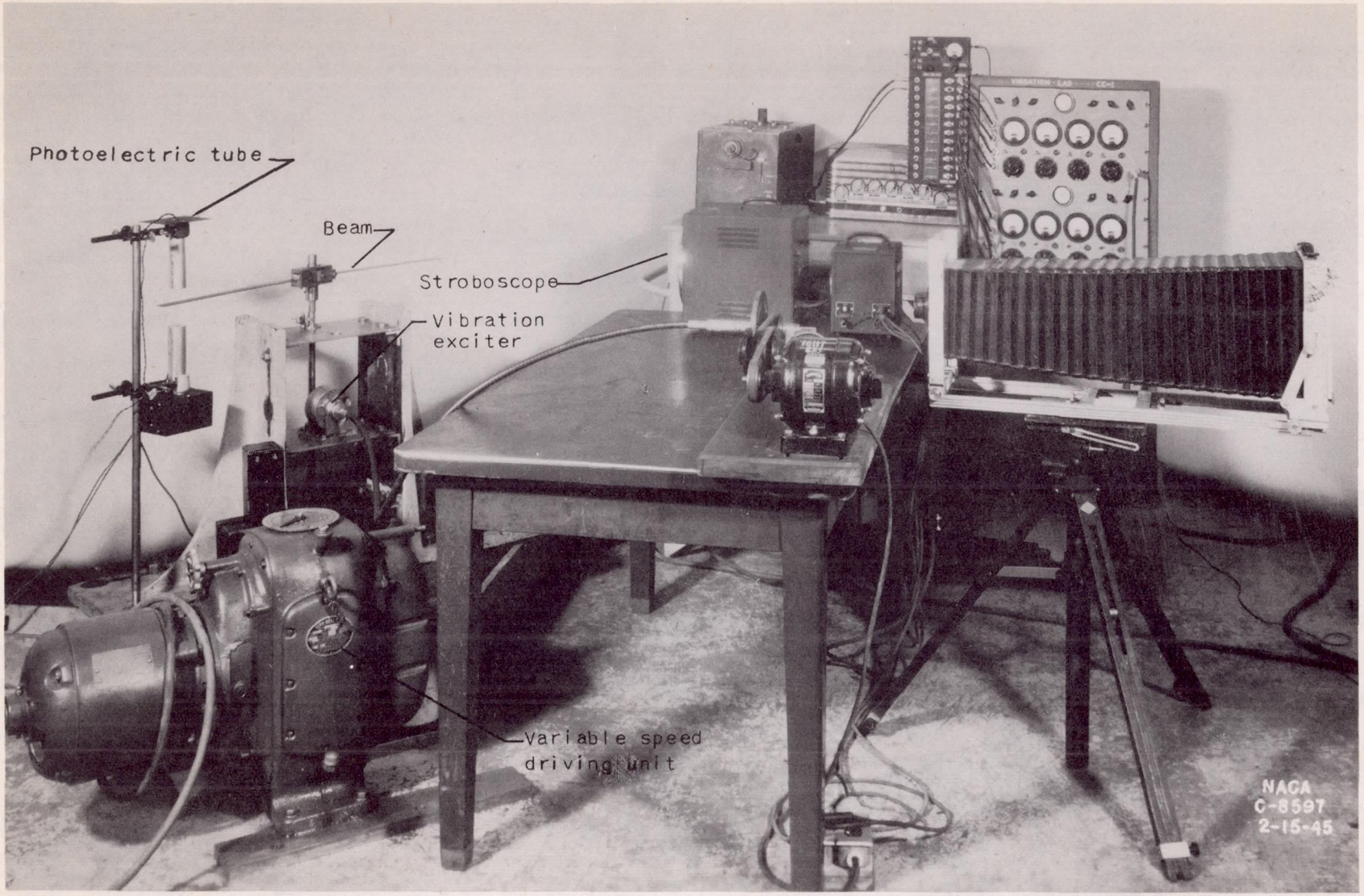

Figure 4. - Test setup for taking stroboscopic photographs of rotating beam.

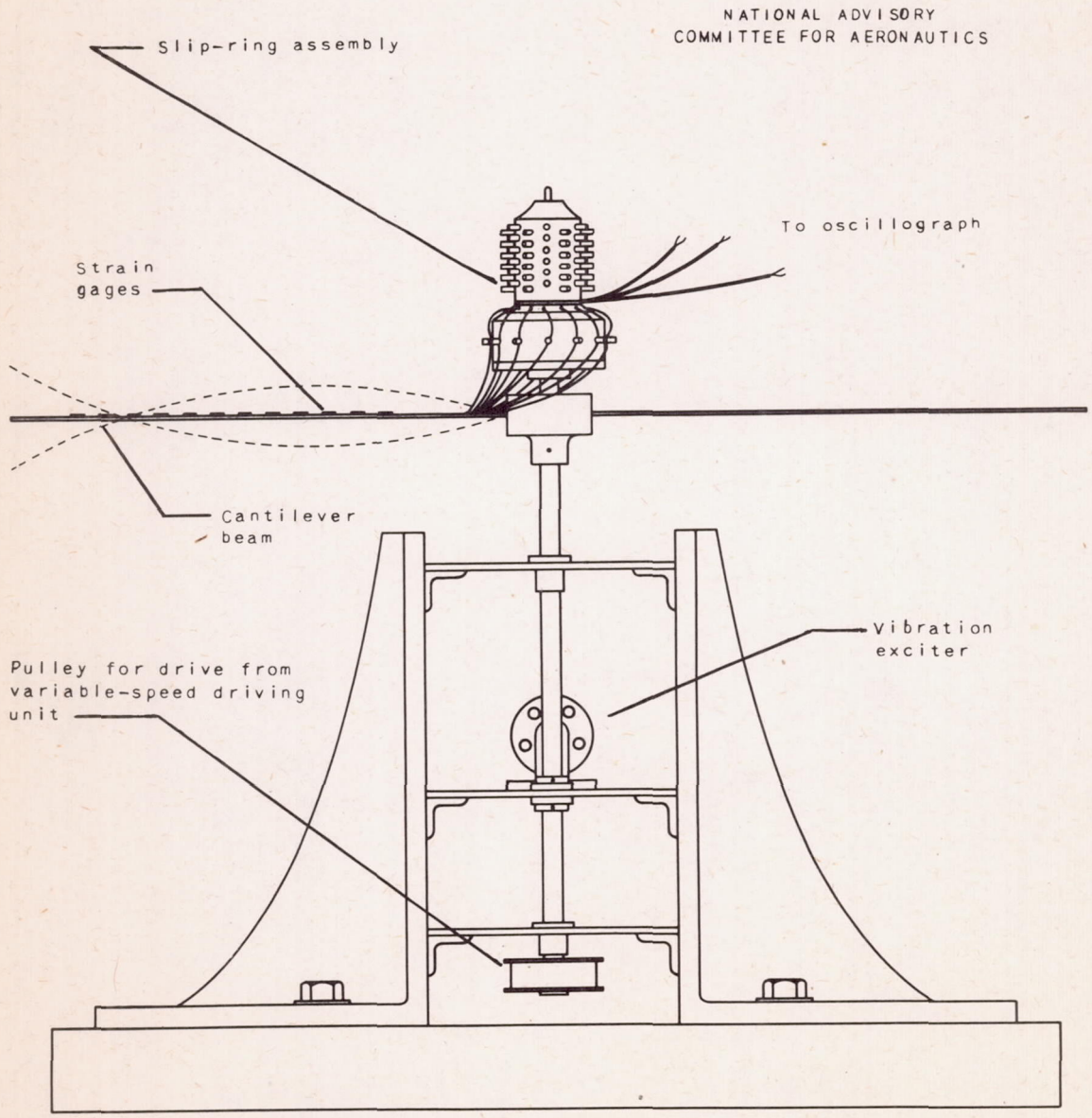

Figure 5. - Diagrammatic sketch of setup for measuring vibratory stress along cantilever beam that is simultaneously rotating and vibrating.

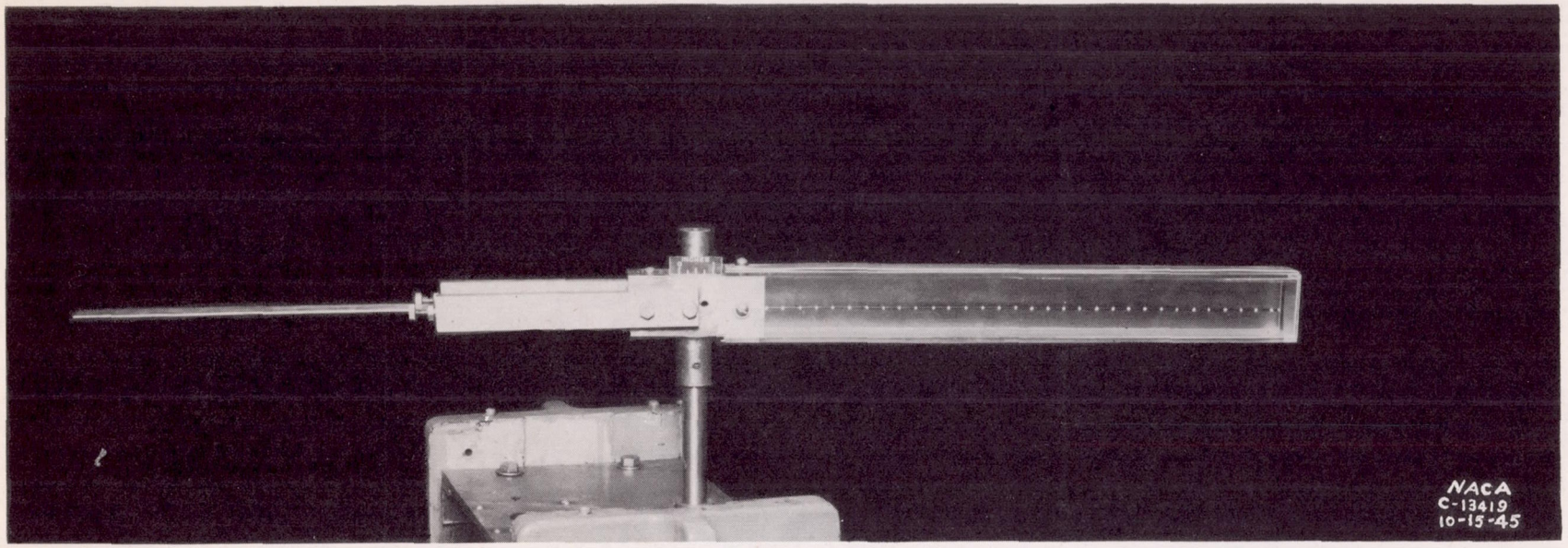

Figure 6. - Cantilever beam enclosed in plastic box to eliminate rotational aerodynamic damping effect.

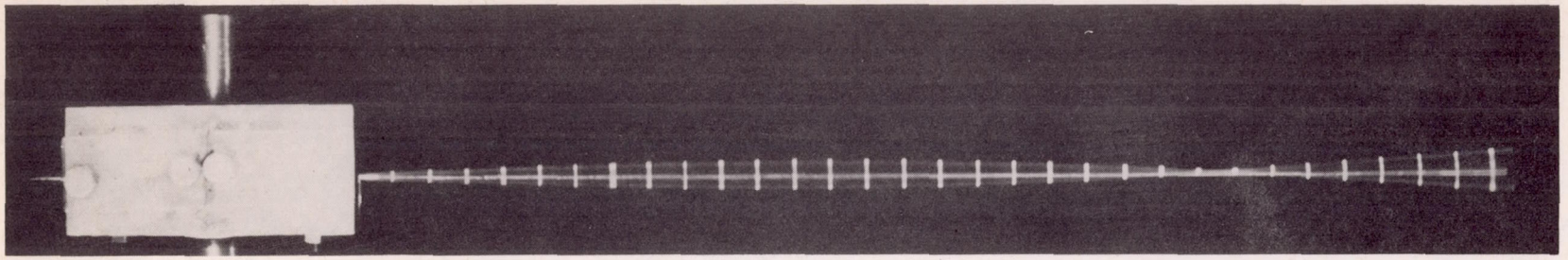

(a) Rotational speed, 1015 rpm; frequency, 57.9 cycles per second.

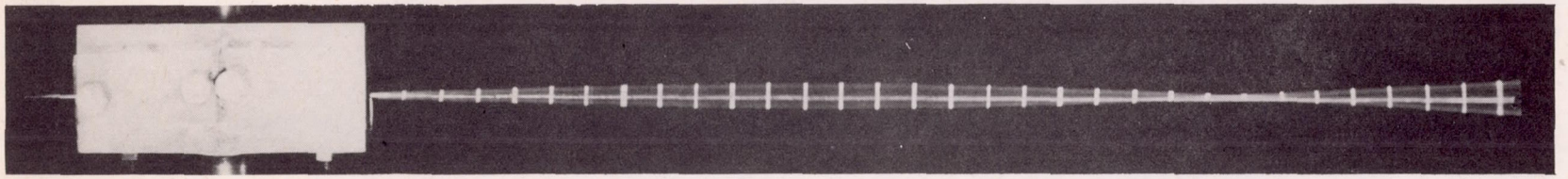

(b) Rotational speed, 536 rpm; frequency, 44.7 cycles per second.

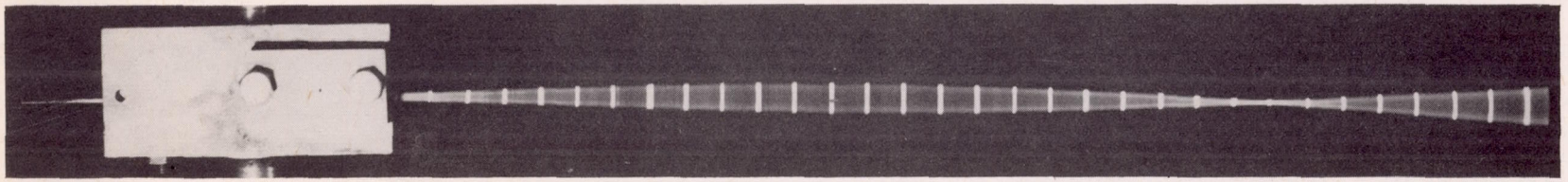

(c) Rotational speed, 0 rpm; frequency, 38.6 cycles per second.

NACA
C-15801
9-6-46

Figure 7. - Stroboscopic photographs of uniform cantilever steel beam fixed at center of rotation and vibrating in second mode at various speeds of rotation.

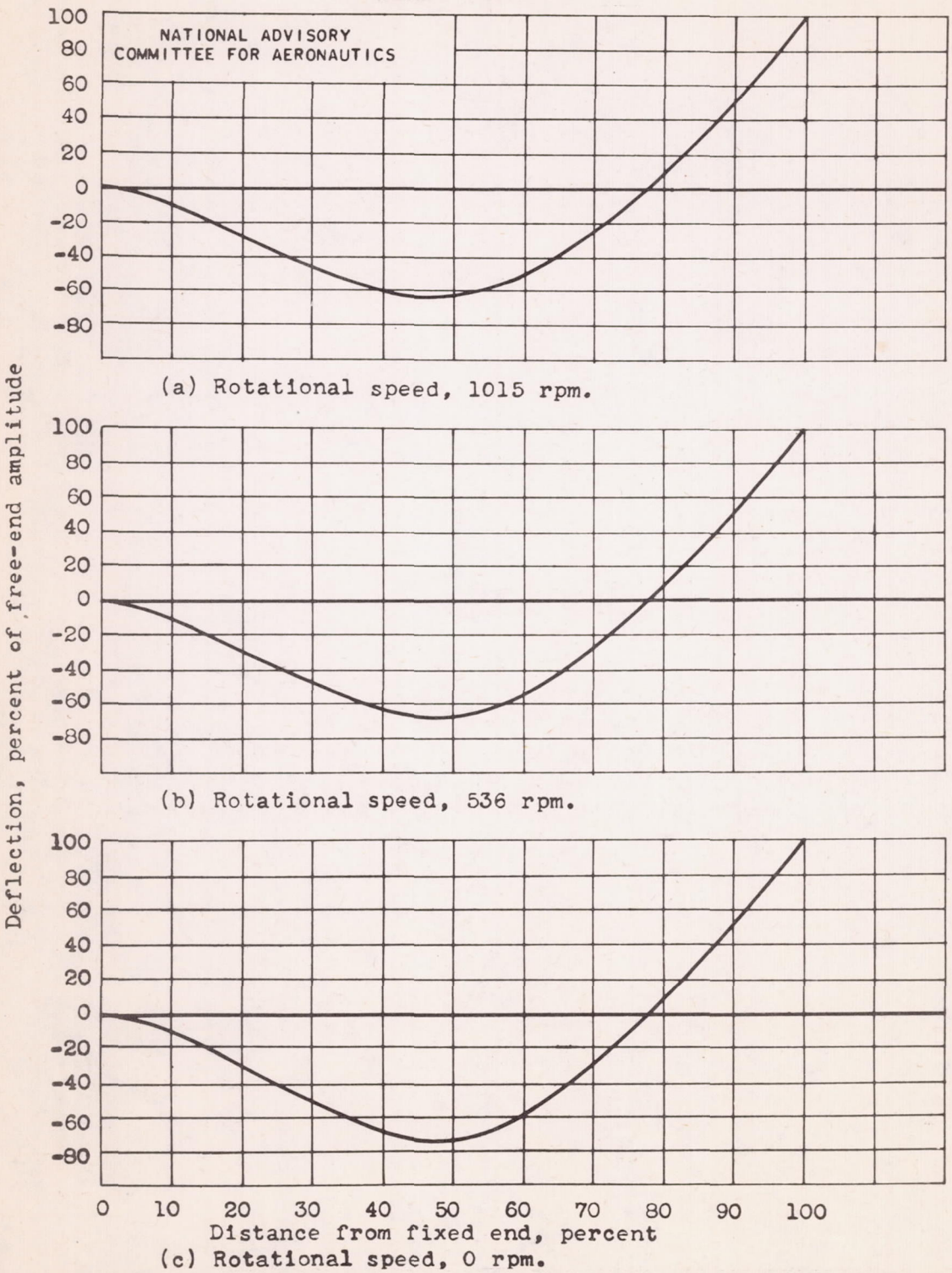

(a) Rotational speed, 1015 rpm.

(b) Rotational speed, 536 rpm.

(c) Rotational speed, 0 rpm.

Figure 8. - Experimental deflection curves of uniform cantilever steel beam fixed at center of rotation and vibrating in second mode while rotating at various speeds.

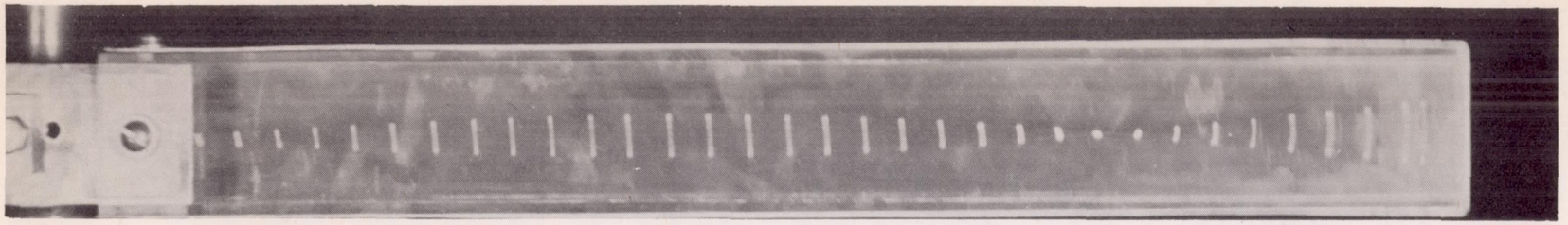

(a) Rotational speed, 1015 rpm; frequency, 57.9 cycles per second.

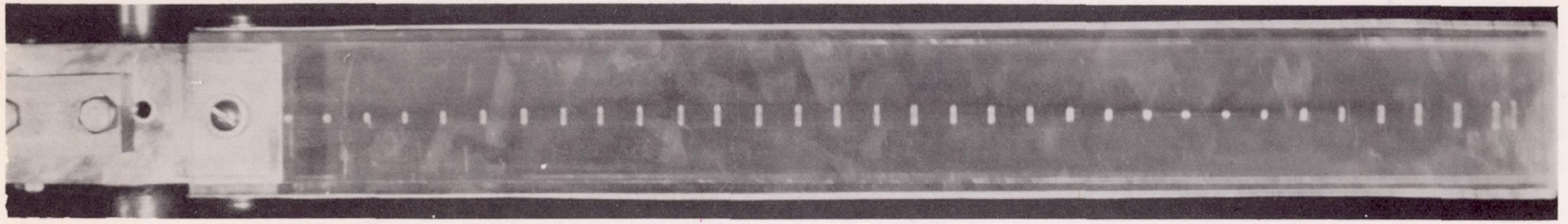

(b) Rotational speed, 536 rpm; frequency, 44.7 cycles per second.

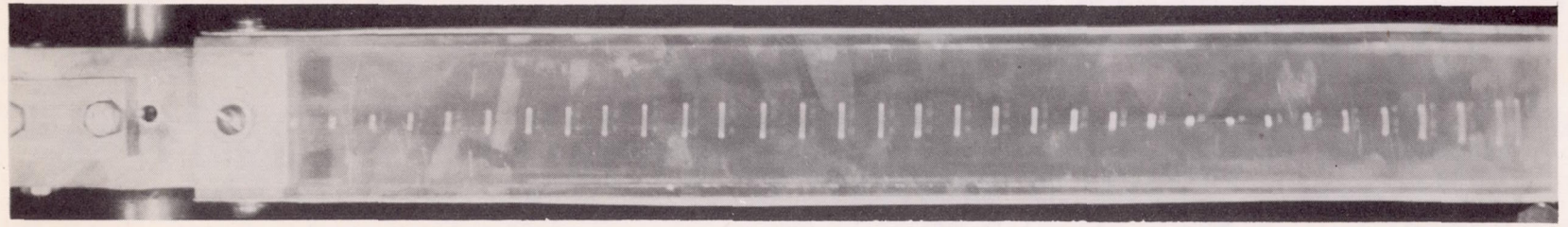

(c) Rotational speed, 0 rpm; frequency, 38.6 cycles per second.

NACA
C-15802
9-6-46

Figure 9. - Stroboscopic photographs of uniform cantilever steel beam enclosed in transparent plastic box fixed at center of rotation and vibrating in second mode at various speeds of rotation.

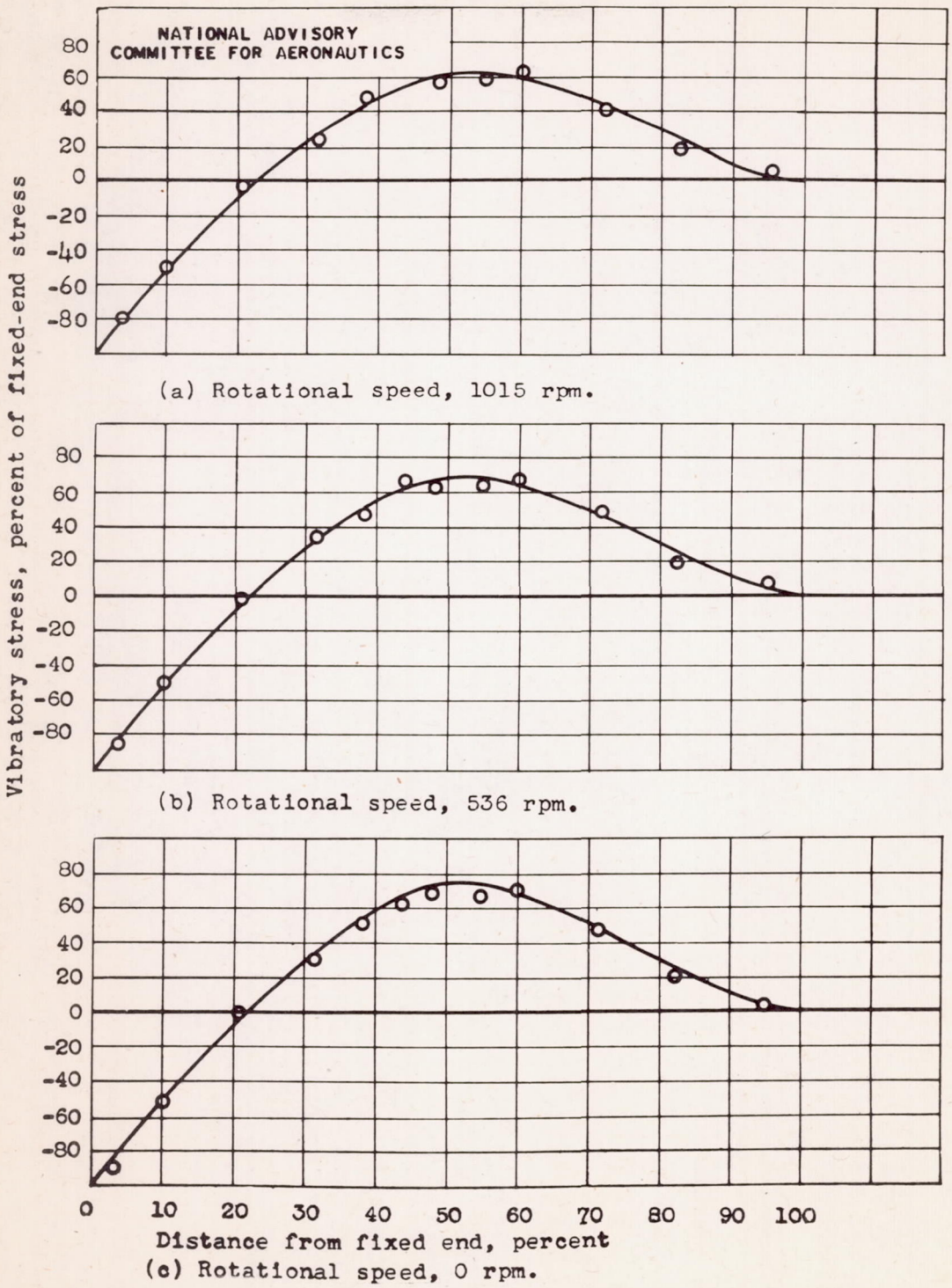

(a) Rotational speed, 1015 rpm.

(b) Rotational speed, 536 rpm.

(c) Rotational speed, 0 rpm.

Figure 10. - Vibratory stress-distribution curves of uniform cantilever steel beam fixed at center of rotation and vibrating in second mode while rotating at various speeds. Stress curves drawn from second derivative of experimental deflection curves of figure 8. Experimental points obtained from strain-gage readings.

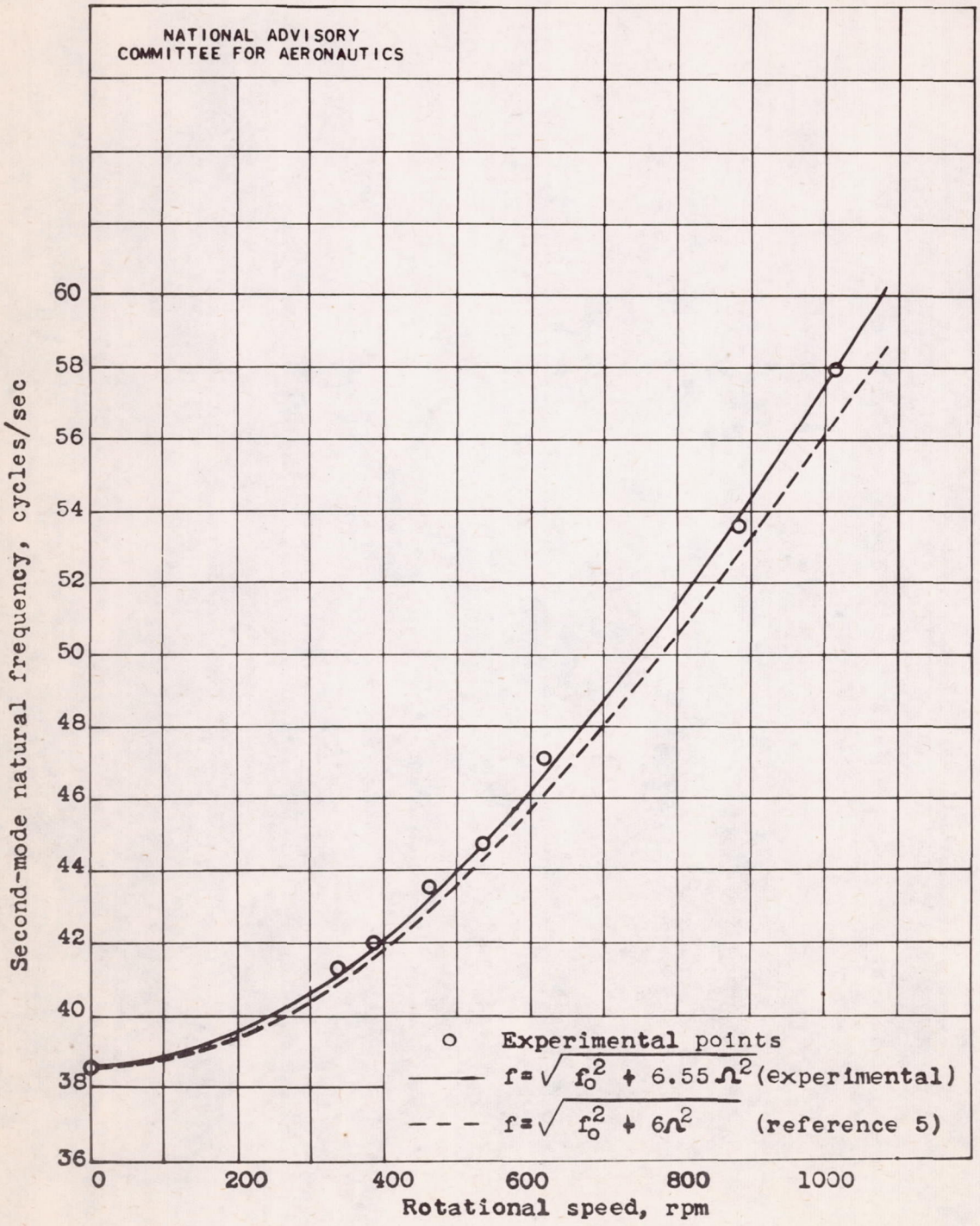

Figure 11. - Variation of second-mode natural frequency with rotational speed for uniform cantilever steel beam, 1/16 inch deep, 1 inch across, and $17\frac{13}{16}$ inches long with fixed end at center of rotation.

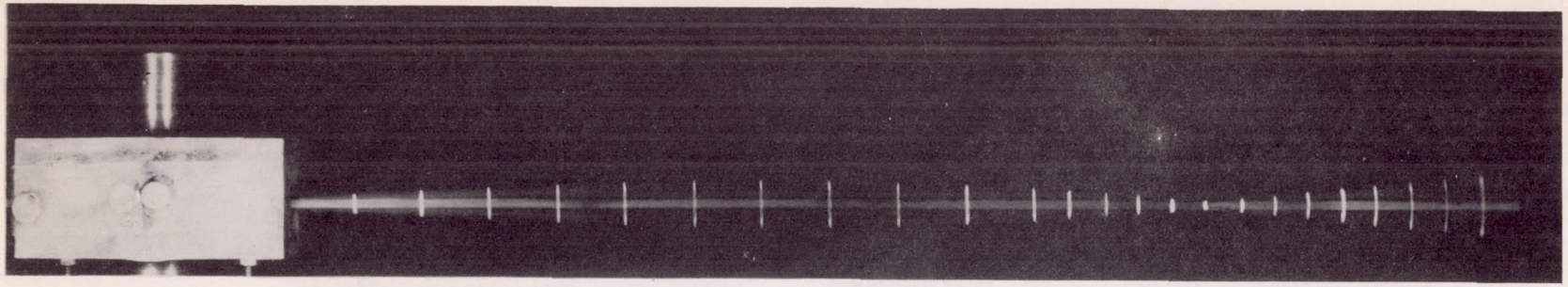

(a) Rotational speed, 998 rpm; frequency, 60.2 cycles per second.

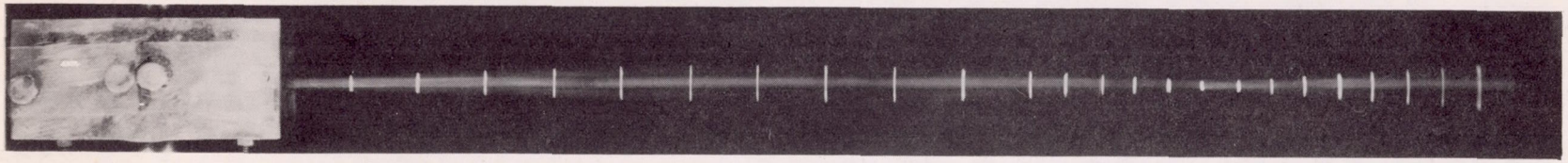

(b) Rotational speed, 525 rpm; frequency, 48.3 cycles per second.

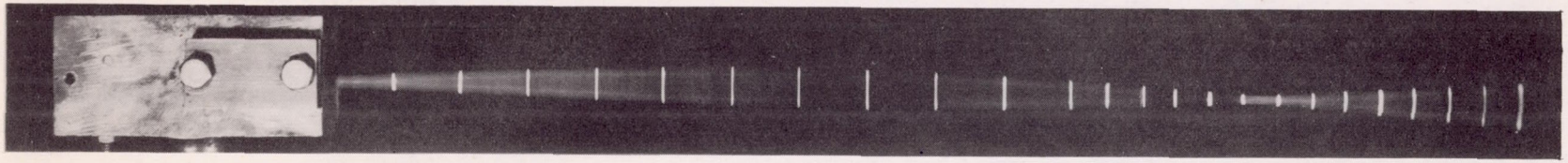

(c) Rotational speed, 0 rpm; frequency, 42.5 cycles per second.

NACA
C-15803
9-6-46

Figure 12. - Stroboscopic photographs of uniform cantilever brass beam fixed at center of rotation and vibrating in second mode at various speeds of rotation.

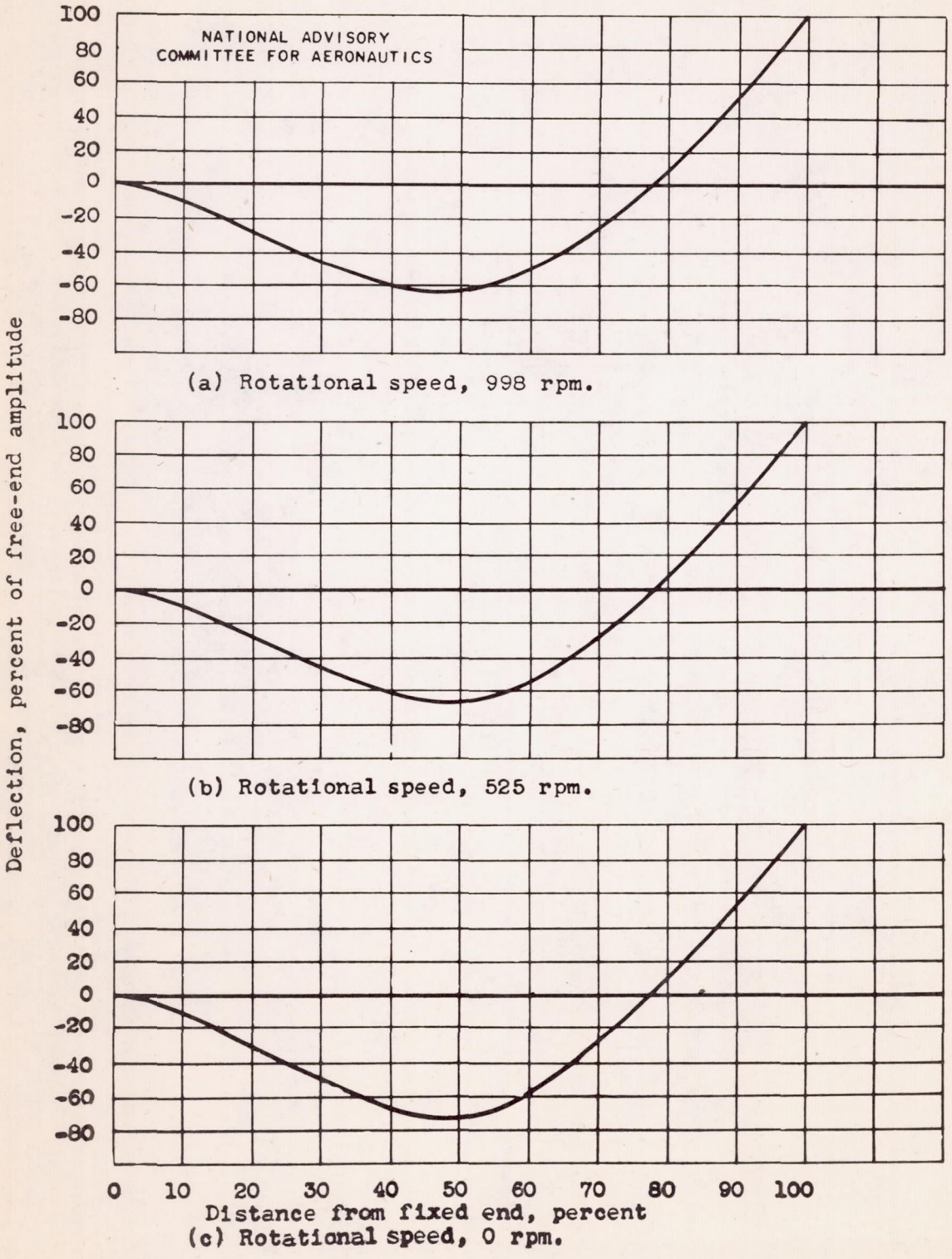

Figure 13. - Experimental deflection curves of uniform cantilever brass beam fixed at center of rotation and vibrating in second mode while rotating at various speeds.

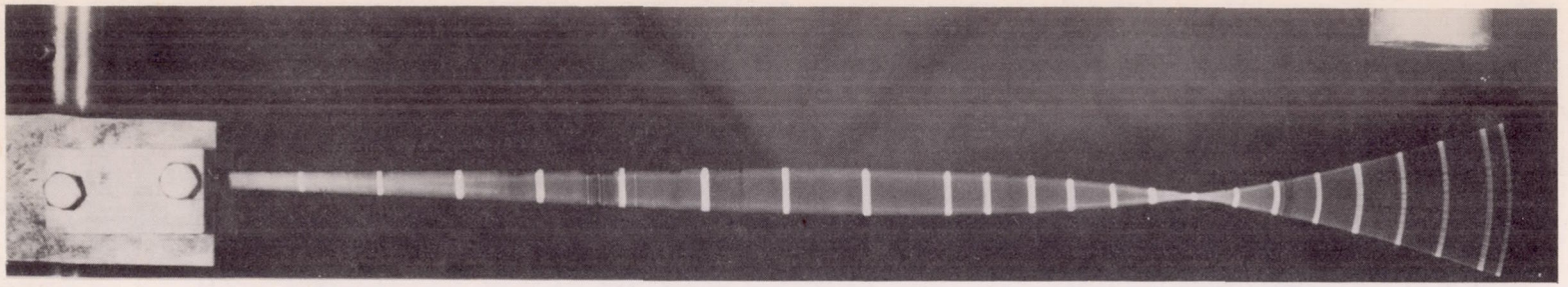

(a) Rotational speed, 1010 rpm; frequency, 86.7 cycles per second.

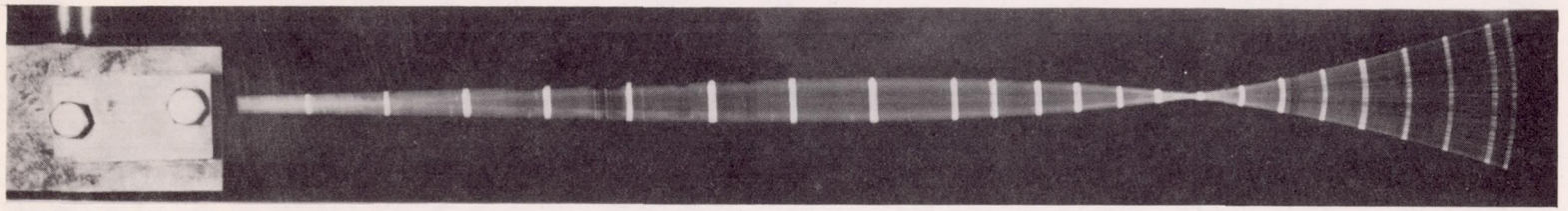

(b) Rotational speed, 503 rpm; frequency, 81.7 cycles per second.

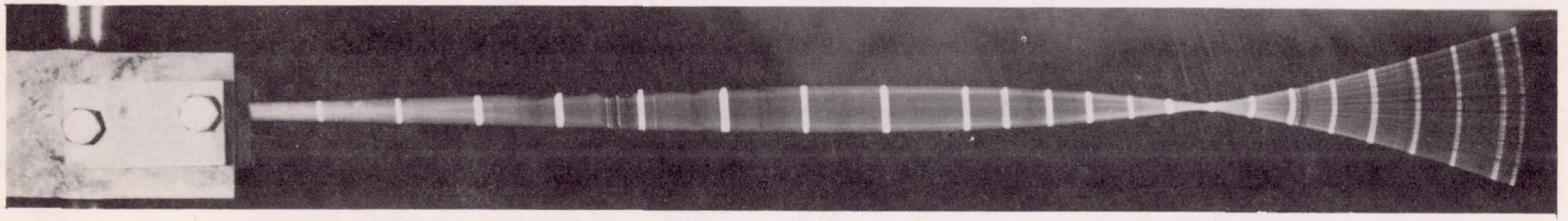

(c) Rotational speed, 0 rpm; frequency, 80 cycles per second.

NACA
C-15804
9-6-46

Figure 14. - Stroboscopic photographs of tapered cantilever steel beam fixed at center of rotation and vibrating in second mode at various speeds of rotation.

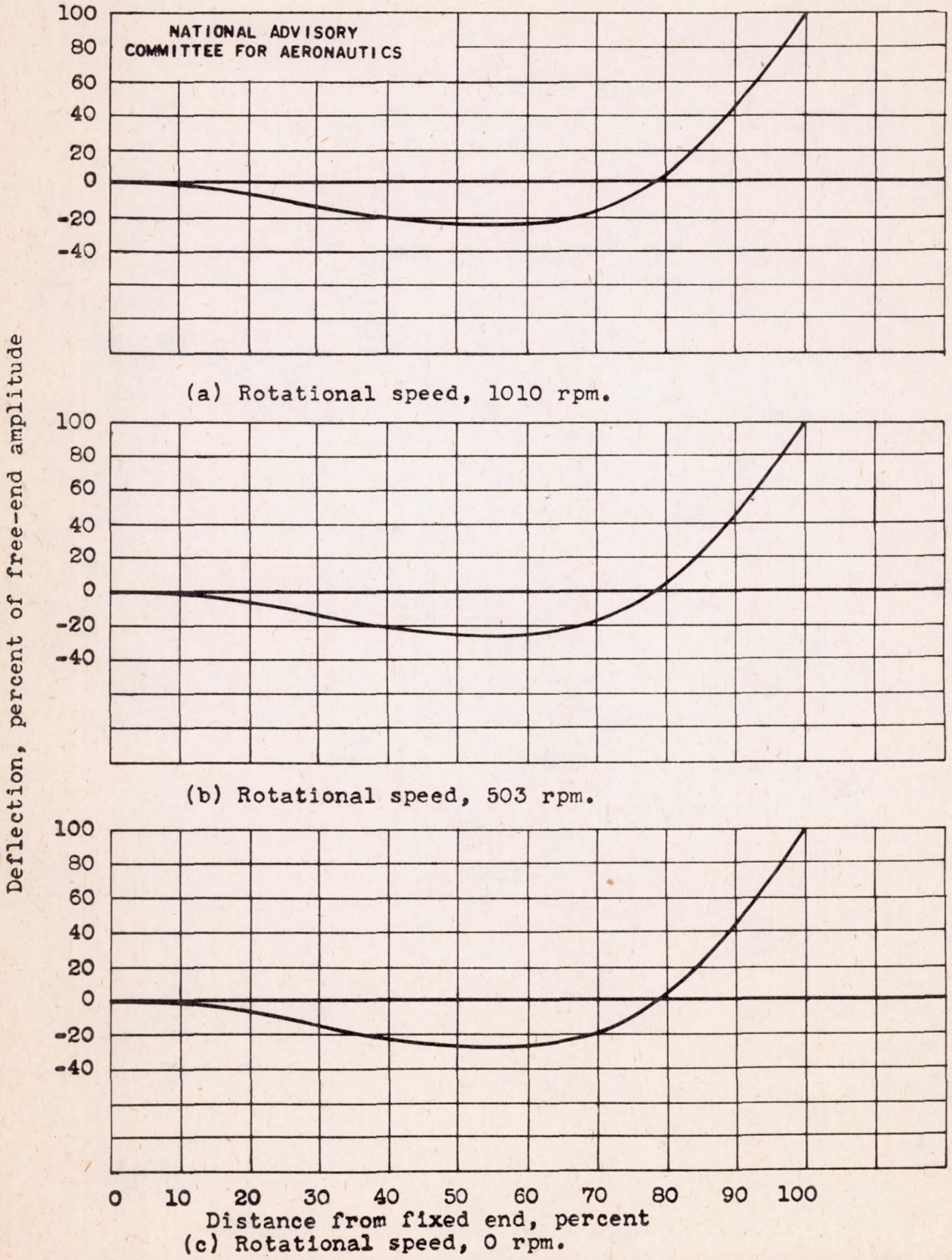

(a) Rotational speed, 1010 rpm.

(b) Rotational speed, 503 rpm.

(c) Rotational speed, 0 rpm.

Figure 15. - Experimental deflection curves of tapered cantilever steel beam fixed at center of rotation and vibrating in second mode while rotating at various speeds.

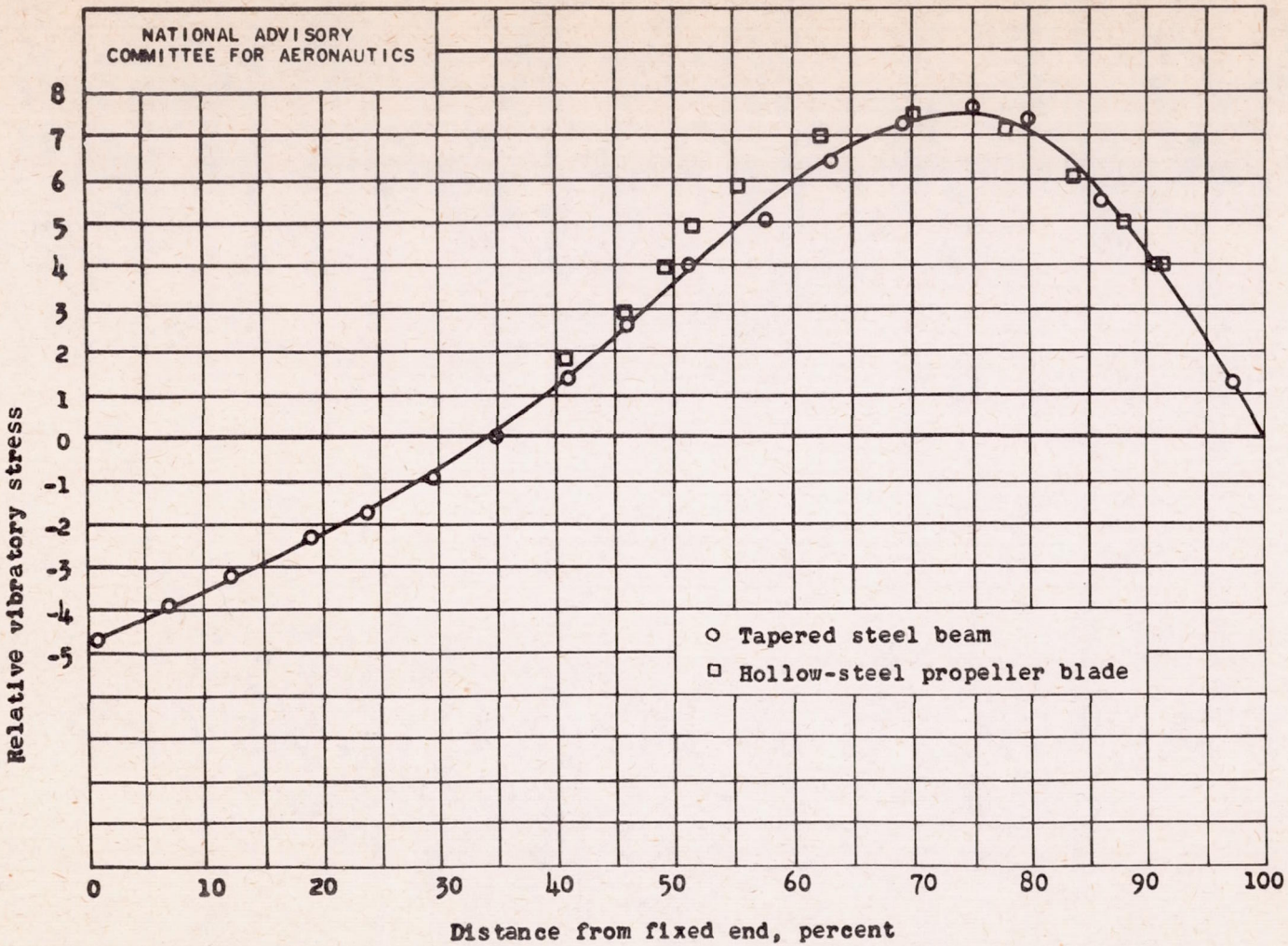

Figure 16. - Comparison of stress distribution along tapered cantilever steel beam and hollow steel propeller blade. Stress curve drawn from second derivative of experimental deflection curve (fig. 15(c)) of tapered cantilever steel beam. Experimental points obtained from strain-gage readings.

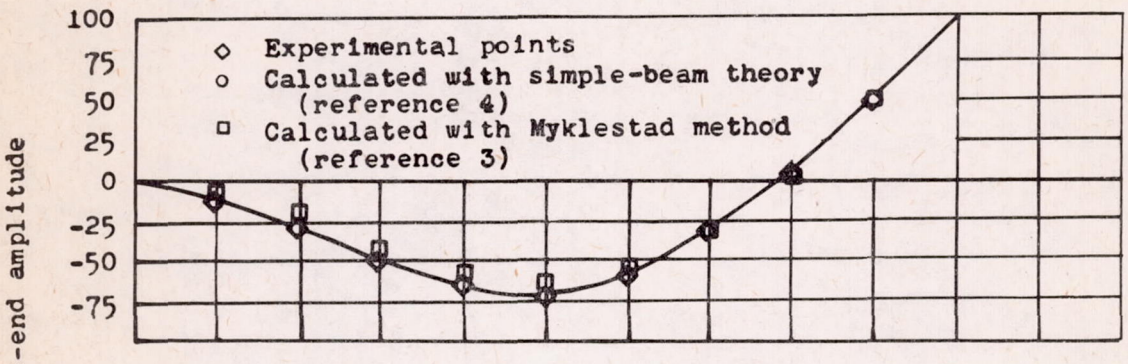

(a) Angular frequency ratio, 0.

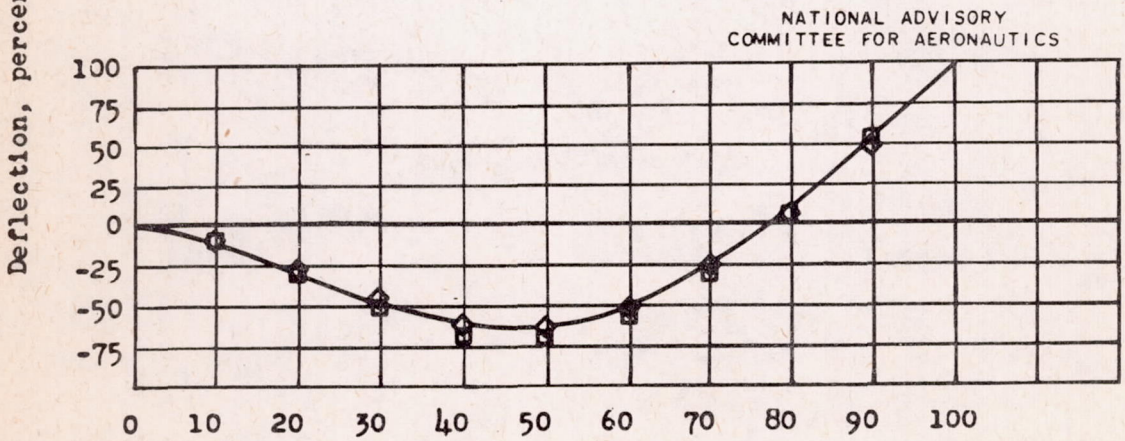

(b) Angular frequency ratio, 0.292.

Figure 17. - Comparison of theoretical and experimental curves showing second-mode deflections of uniform cantilever beam for two rotations.